Aerosevoelastic Design Definition of a 20 MW Common Research Wind Turbine Model

T. Ashuri[a,1,*], J. R. R. A. Martins[b,2], M. B. Zaaijer[c,3], G. A. M. van Kuik[c,2], G. J. W. van Bussel[c,2]

[a] *University of Texas at Dallas, Department of Mechanical Engineering, Richardson, 75080 TX, USA*

[b] *University of Michigan, Department of Aerospace Engineering, Ann Arbor, 48109 MI, USA*

[c] *Delft University of Technology, Department of Aerodynamics and Wind Energy, Kluyverweg 1, Delft, 2629 HS, The Netherlands*

Abstract

Wind turbine upscaling is motivated by the fact that larger machines can achieve lower levelized cost of energy. However, there are several fundamental issues with the design of such turbines, and there is little public data available for large wind turbine studies. To address this need, we develop a 20 MW common research wind turbine design that is available to public [1]. Multidisciplinary design optimization is used to define the aeroservoelastic design of the rotor and tower subject to the following constraints: blade-tower clearance, stresses, modal frequencies, tip-speed and fatigue damage at several sections of the tower and blade. For blade the design variables include blade length, twist and chord distribution, structural thicknesses distribution and rotor speed at the rated. The tower design variables are the height, and the diameter distribution in the vertical direction. For the other components, mass models are employed to capture their dynamic interactions. The associated cost of these components is obtained by using cost models. The design objective is to minimize the levelized cost of energy. The results of this research show the feasibility of a 20 MW wind turbine, and provide a model with the corresponding data for wind energy researchers to use in the investigation of different aspects of wind turbine design and upscaling.

Keywords: Wind turbine aeroservoelasticity, multidisciplinary design optimization, common research wind turbine model, 20 MW design, upscaling.

---

[*] Corresponding author

Email address: turaj.ashuri@utdallas.edu (T. Ashuri)

[1] Visiting assistant professor

[2] Professor

[3] Assistant professor

[1] https://github.com/tashuri/20MW-windturbine-model

1. Introduction

Over the last decades, the size of wind turbines experienced a continuous increase in hope of achieving a lower levelized cost of energy (LCoE). Political issues, public acceptance, and the desire of some countries to generate the bulk of their electricity from wind energy are among other factors that support the design of larger units. However, the progressive upscaling of wind turbines poses several technical and economical design challenges that have to be identified and solved.

There are few research studies addressing different aspects of wind turbine upscaling beyond the existing 5–7 MW range [4]. Bak et al. [1] presented the design of a 10 MW upwind, three-bladed, variable-speed, pitch-regulated wind turbine as part of the Light Rotor project. CFD simulations were performed on the rotor to obtain the detailed aerodynamics characteristic for aeroelastic simulations [2]. Peeringa et al. [3] presented a pre-design of a 20 MW turbine including the controller. Here, first a 20 MW design is obtained using linear upscaling of the 5 MW UpWind design [4]. Then, the aerodynamic and structural design of the blade takes place sequentially. A controller is designed after freezing the aerodynamic and structural design of the blade.

The Norwegian research center for offshore wind technology (NOWITECH) developed a 10 MW variable speed, variable pitch turbine with direct-drive permanent magnet synchronous generator coupled to the grid through a fully rated converter [5]. The characteristics of the control strategy, the generator, and the tower are also given, and the integrity of the complete model is demonstrated using aeroelastic simulations [6, 7, 8, 9]. Vatne [10] and Frøyd et al. [11] performed aeroelastic stability analysis of the NOWITECH 10 MW rotor.

Cox and Echtermeyer [12] performed the structural design of a 70 m blade, 10 MW turbine for an upwind horizontal-axis wind turbine. The composite structure of the blade used glass and carbon fiber. Structural analysis studies demonstrated its ability to withstand the extreme loading conditions. Griffith and Ashwill [13] created the design of a 100 m blade for a horizontal axis wind turbine corresponding to 13.2 MW power output. This initial blade was made of fiber-glass with conventional architecture [5], followed by investigation of carbon fiber materials [14], advanced core material design [15], and advanced geometry effects [16]. Loth et al. [17] presented a 13.2 MW downwind rotor concept that uses coning and curvature to align the non-circumferential loads for a given steady-state condition.

A current issue that is preventing the research community to advance the state-of-the-art in large wind turbines is the fact that almost no public information is available about such turbines. Wind turbine manufacturers understandably prefer to keep the designs and data they produce confidential to protect any technological and knowledge

[4]The existing installation size are 5 to 7 MW, and 7 to 8 MW turbines are currently being designed.

[5]A conventional architecture is a blade with a beam box that has two shear webs and two spar caps.

advantage they might have. Therefore, there is a need for a publicly available large scale wind turbine design with the corresponding data for research projects. Such data could also help answer some of the questions in wind turbine design today, namely: (1) How large can we scale up a complete wind turbine (not just a single component), (2) What would be the design characteristics of a large wind turbine?, and (3) What would be an accurate estimate of the LCoE for larger turbines using the current technology?

To address these needs, we developed a 20 MW common research wind turbine complete model and made it publicly available [6]. Unlike the previous studies, the design of this large wind turbine is performed using multidisciplinary design optimization (MDO), a well established design technique for the design of wind turbines [18]. The scaling law provides design for which there is no guarantee of feasibility. Furthermore, even if feasible, a scaled design will not be an optimal design solution. Therefore, the MDO methodology used in this research provides a feasible and optimum design for the 20 MW turbine.

Since active control is becoming increasingly important for larger wind turbines, this work extends the previous optimization studies with no controller or a fixed controller strategy by updating controller parameters during every optimization iteration [18, 19, 20, 21, 22, 23, 24]. The integrated design of a controller enables the development of an economically more attractive large scale wind turbine by increasing energy capture using a controller that is optimized simultaneously with the rest of the design.

The majority of large scale wind turbines designed nowadays are upwind, three-bladed, pitch-regulated, variable-speed turbines, and this is the focus of this research as well. To provide an initial set of design variables needed for the optimization to start with, the 5 MW UpWind [4] wind turbine design data are upscaled to a 20 MW design using scaling rules [25], and a scaling factor of two. After this step, optimization of the design takes place to provide the optimal preliminary data, such as rotor diameter, hub height, rated rotational speed, and structural and aerodynamic design of the tower and rotor.

To evaluate the LCoE as the design objective function, various components of the cost breakdown and the annual energy production (AEP) are needed. For several components of the cost breakdown, the WindPACT [26] heuristic cost models have been used. However, for the tower and rotor blade these cost models have not been used. Instead, the design variables of the tower and blade structures, such as the tower wall thickness and rotor chord are optimized. The cost contributions of these components to the LCoE are determined from the design variables' values. In particular, the mass is determined from the design variables and the costs are calculated from the mass. This approach gives the cost evaluation a much wider range of applicability than the heuristic, data dependent models. However, although the tower and blades are parametrically optimized for the 20 MW scale, their concept and configuration are similar to those of current multi-megawatt turbines.

[6] `https://github.com/tashuri/20MW-wind-turbine-model`

These cost and mass models are either dependent or independent of the blade and tower design variables. Therefore, during the optimization process, the value of these dependent models is also adjusted to give an integrated design with the lowest LCoE. An example of a dependent model is the hub mass and cost, which depends on the blade mass. The independent models do not have any size dependency, and are therefore fixed for all sizes. The cost of the safety system is an example of a model that is independent of the size. Details of these models can be found in previous works [27, 28, 29, 30, 31], and are therefore not discussed here.

The quantification of the AEP, the system masses, and the costs allows the LCoE to be calculated and used as a multidisciplinary objective function to be minimized. The solution of this optimization problem results a wind turbine design that includes rotor and tower data, cost and mass data, and the operational parameters of the wind turbine. The optimization is done for wind conditions at a Dutch site [32].

2. MDO formulation

To formulate a MDO problem, the choice of an optimization architecture, design variables and constraints, objective function and optimization algorithm needs to be defined. An architecture integrates the aeroservoelastic analysis method (to simulate the system under study) with optimizer, and it defines the data flow and computational process. This section outlines the MDO formulation, while the next section presents the aeroservoelastic analysis method.

2.1. Optimization architecture

Among the various optimization architectures described in the literature [33], this study uses multidisciplinary feasible design (MDF) architecture. In MDF, the optimizer is directly linked to the disciplinary solvers as depicted in Figure 1 using the extended design structure matrix (XDSM)convention [34]. The disciplinary solvers shown in this figure are described in Section 3.1.

2.2. Design variables

The 20 MW wind turbine developed in this research has the following design features:

1. A three-bladed upwind rotor attached to a conical hub with 3 m/s cut-in and 25 m/s cut-out wind speed.
2. A collective PI pitch-to-feather controller for power regulation above the rated.
3. A variable-speed generator torque controller for energy maximization below the rated.
4. A geared drive train with a full converter.
5. A minimum of 25 m air-gap between the unloaded blade-tip and the ground.
6. A tubular tower concept nonlinearly tapered from the bottom to top.

To obtain the initial set of design variables needed for the optimization to start with, the 5 MW UpWind wind turbine developed in the framework of the UpWind

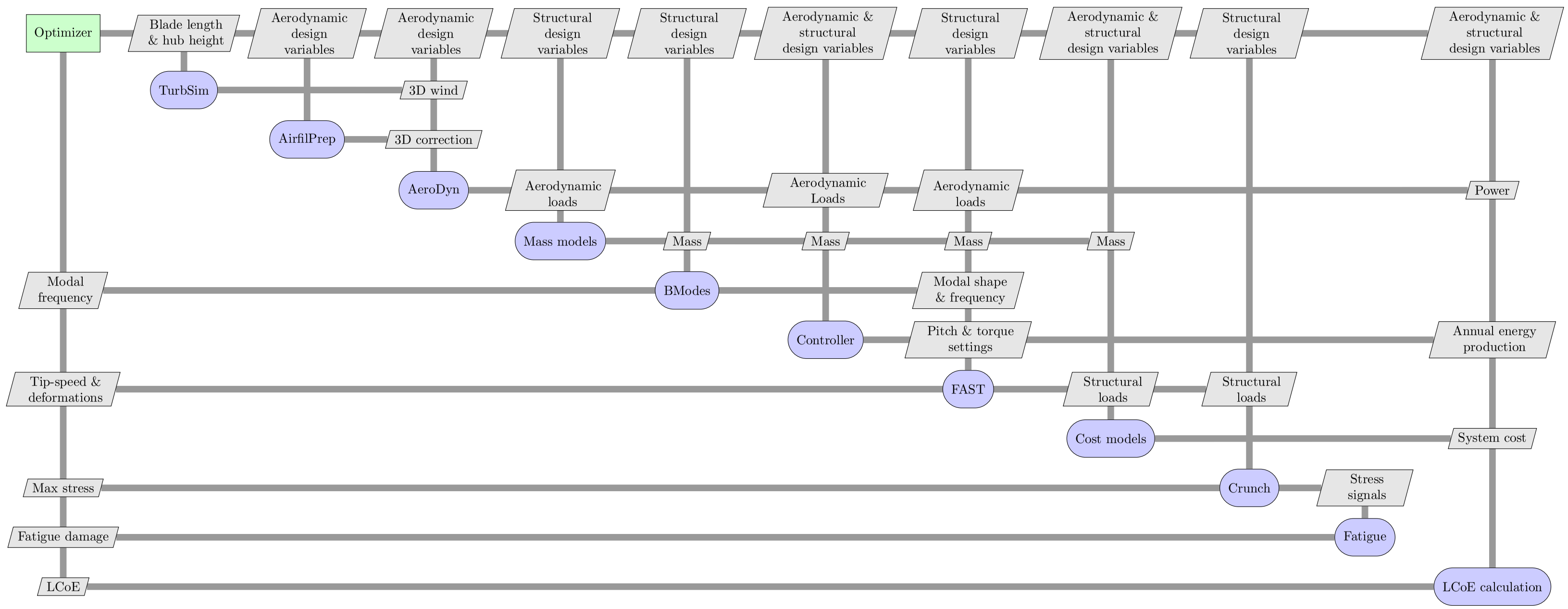

Figure 1: Extended design structure matrix (XDSM)[34] describing the how the computational codes and the optimizer are coupled. The top parallelograms are the data passed to the codes, and the lines represent the data dependencies. The optimizer is located in the top green box, and the computational codes are the blue boxes. The data flow on the upper triangular is from left to right, and top to bottom, and on the lower triangular is from right to left, and bottom to top.

project is linearly upscaled by factor of two as in Nijssen et al. [35]. Table 1 lists the design variables for the 20 MW wind turbine. This table also defines the bounds of the design variables (lower and upper bounds) needed to define the design space. The choice of the optimization level is related to the way these design variables are optimized and further explained in Section 2.4.1.

Table 1: Blade and tower design variables for the initial and optimal designs, with corresponding upper and lower limits

Variable (units)	Opt. level	Lower	Initial	Optimal	Upper
Length of blade (m)	1	110.0	123.0	135.0	140.0
Height of tower (m)	1	150.0	175.2	155.0	190.0
Rotational speed at rated (rpm)	1	6.0	6.4	7.1	7.5
Section 6, twist (deg)	2	10.0	13.3	14.8	15.0
Section 10, twist (deg)	2	5.0	10.2	5.8	11.0
Section 14, twist (deg)	2	2.0	3.3	3.1	5.0
Section 17, twist (deg)	2	0.0	0.4	1.5	3.0
Section 20, twist (deg)	2	0.0	0.0	0.1	2.0
Section 1, chord (m)	2	6.0	7.1	7.6	8.0
Section 6, chord (m)	2	7.0	9.1	10.0	10.0
Section 10, chord (m)	2	6.0	8.0	6.7	9.0
Section 17, chord (m)	2	2.0	4.6	2.9	6.0
Section 20, chord (m)	2	0.1	0.2	1.6	2.5
Section 1, skin thickness (cm)	2	18.0	20.0	19.0	21.0
Section 3, skin thickness (cm)	2	10.0	12.0	18.9	21.0
Section 6, skin thickness (cm)	2	4.0	4.6	17.1	20.0
Section 16, skin thickness (cm)	2	2.0	3.0	16.2	20.0
Section 3, web thickness (cm)	2	1.5	2.0	14.5	20.0
Section 6, web thickness (cm)	2	2.0	4.0	16.0	20.0
Section 16, web thickness (cm)	2	2.0	2.6	15.2	20.0
Section 3, spar thickness (cm)	2	1.0	2.0	14.4	20.0
Section 6, spar thickness (cm)	2	1.0	5.0	13.2	20.0
Section 16, spar thickness (cm)	2	1.0	4.8	10.0	20.0
Section 1, tower diameter (m)	2	9.0	12.0	10.0	15.0
Section 7, tower diameter (m)	2	8.0	12.0	9.0	15.0
Section 14, tower diameter (m)	2	6.0	9.8	6.9	12.0
Section 22, tower diameter (m)	2	5.0	8.2	6.2	10.0

There are 22 design variables for the rotor. These variables are the external geometry (11), structural thickness (10), and rotor rotational speed (1). The geometry variables are 5 chord lengths at section 1 (blade root), 6, 10, 17 and 20 (blade tip), blade length, and 5 twist angles at section 6, 10, 14, 17 and 20. The structural thicknesses of the composite lay-ups are 3 spar thicknesses at section 3, 6 and 16, 4 shell thicknesses at section 1, 3, 6, 16, and 3 web thicknesses at section 3, 6 and 16. The rotational speed of the rotor and the blade length together define the tip-speed of the blade, which is considered as a design constraint.

The five design variables of the tower are the tower height (1), and the diameter at sections 1 (tower bottom), 7, 14 and 22 (tower top). We assumed a fixed diameter to thickness ratio of 160 to find the value of thickness at the sections where the diameter optimization takes place. This is common practice in the oil and gas industry to design against pile buckling at the conceptual and preliminary design phases [36, 37]. This design variable linking technique not only reduces the computational time, but also prevents buckling. All these design variables are continuous.

Table 6 lists the exact locations of each blade section, and Table 14 list the locations for the tower sections. For the blade, these sections are measured from the blade root (section 1) to the tip (section 20), and for the tower they start at the tower bottom (section 1) and end up at the tower top (section 22). Cubic interpolation is employed to find the distributed properties of the blade and tower between these sections. To have a smooth and continuous interpolation of the section design variables, the following parameters are predefined:

1. Sections 1 to 3 (root region) have a circular cross section with equal diameter for these sections.
2. The twists for sections 1 trough 6 are equal. These sections serve to transition from the circular root section to an airfoil shape, and they do not contribute in a significant way to power generation.
3. Shear web and cap thicknesses close to the blade root (sections 1 and 2) are zero.

2.3. Design constraints

Several inequality constraints are used to obtain a feasible design solution of the blade and tower as detailed in Tables 2 and 3. The design constraints of the blade are fatigue damage at five sections along the blade, stresses, blade-tower clearance, and the first three natural frequencies. The design constraints of the tower are fatigue damage and stress at six sections along the tower, and the first and second natural frequencies.

Partial safety factors are used in combination with these constraints to cover the design and modeling uncertainties. Table 4 shows the selected values for the partial safety factors, except for the design load case 2.3 (see Table 8), where a partial safety factor of 1.1 for the ultimate limit state is used.

2.4. Objective function

LCoE is a representative multidisciplinary objective function that reflects the trade-offs between all disciplines, and results in a true assessment of all the technical and economical changes. For a single wind turbine operating in a wind farm, LCoE contains

Table 2: Turbine blade design constraints (accounting for safety factors)

Constraint	Value (units)
Tip-deflection	≤ 18.3 (m)
Section 1, 3, 6, 10, 17, 20 flapwise fatigue	≤ 0.7 (–)
Section 1, 3, 6, 10, 17, 20 edgewise fatigue	≤ 0.7 (–)
Section 1, 3, 6, 10, 17, 20 flapwise stress	≤ 276 (MPa)
Section 1, 3, 6, 10, 17, 20 edgewise stress	≤ 276 (MPa)
1$^{\text{st}}$ frequency	$2.1P \leq \omega_{1n} \leq 2.9P$ (Hz)
2$^{\text{nd}}$ frequency	$\omega_{2n} \geq 3.1P$ (Hz)
3$^{\text{rd}}$ frequency	$\omega_{3n} \geq 3.1P$ (Hz)
Tip-speed	≤ 120 (m/s)

Table 3: Tower design constraints (accounting for safety factors)

Constraint	Value (units)
Section 1, 5, 9, 13, 17, 21 stress (fore-aft)	≤ 333 (MPa)
Section 1, 5, 9, 13, 17, 21 fatigue damage (fore-aft)	≤ 0.7 (-)
1$^{\text{st}}$ frequency	$1.1P \leq \omega_{1n} \leq 1.9P$ (Hz)
2$^{\text{nd}}$ frequency	$\omega_{1n} \geq 3.1P$ (Hz)

Table 4: Partial safety factors [38]

Type of safety factor	Value
Material	1.05
Failure consequence	Blade 1.0 Tower 1.0
Ultimate limit state	1.35
Fatigue limit state	1.43
Modal frequency	$\pm 0.1P$

the following elements [26]: Turbine capital cost (TCC), balance of station (BOS), initial capital cost (ICC), levelized replacement cost (LRC) and operations and maintenance (OM) costs. Note that in the calculation of the BOS, we did not consider any transportation cost, since the WindPACT model estimates an unrealistically high transportation cost for large wind turbines.

These cost models were calculated based on the cost of materials and products for year 2002, and are adjusted in this research based on the cost of materials and products to account for inflation according to the producer price index [7]. The combination of these cost models and the AEP enables the calculation of LCoE as:

$$\mathrm{LCoE} = \left(\frac{\mathrm{ICC} \times \mathrm{IR} + \mathrm{LRC} + \mathrm{OM}}{\mathrm{AEP}}\right), \tag{1}$$

where IR is the interest rate with a value of 0.118. AEP is the yearly energy production, which can be written as,

$$AEP \approx 8760 \sum_{i=\text{cut-in}}^{\text{cut-out}} P(V_i) f(V_i), \tag{2}$$

where $P(V)$ is the turbine power curve, 8760 is the total number of hours in a year, i is the wind speed index that ranges from the cut-in to cut-out speeds, with an interval of 2 m/s. The wind probability distribution function $f(V)$ is calculated using,

$$f(V) = \left(\frac{k}{c}\right)\left(\frac{V}{c}\right)^{k-1} \exp\left[-\left(\frac{V}{c}\right)^{k}\right], \tag{3}$$

where k is the shape factor, V is the wind speed, and c is the wind speed scale factor. Here, $c = 9.47$ and $k = 2$. An AEP conversion loss of 5.6% is assumed (for the mechanical-to-electrical energy conversion in the drive train), which is the same as the DOWEC design at the rated power [39].

2.4.1. Optimization algorithm and implementation

There are several factors that make the present design optimization computationally expensive: (1) The simultaneous design optimization of the blade and tower with several design variables and constraints; (2) The use of time domain simulation of the wind turbine with multiple design load cases to capture the dynamic behavior, and (3) The required gradients of the objective function and design constraints, which are computed using finite differences. To save computational time, the design variables are decomposed, resulting in a bi-level optimization approach. In both optimization levels, LCoE is minimized but with respect to different sets of variables.

For the first level, the convex linearization (CONLIN) algorithm is used [40]. For the second level of the optimization process, we use the Lagrange multiplier

[7] http://www.bls.gov/ppi/

method [41]. The level one optimization process runs quickly since there is only one design constraint is enforced (the blade tip-speed), and the design variables are only tower height, blade length, and rated rotational speed.

The second level optimization starts with the optimized values from the level one optimized tower height, blade length, and rated rotational speed. All the other design variables are optimized subject to all the design constraints. This iterative process between the two levels continues until the specified convergence of 1% in the LCoE value is achieved. This tolerance is achieved after four iterations of the bi-level optimization, each having 10 to 14 iterations for level 1, and 25 to 32 iterations for level 2. The total optimization time was 1,150 hours of wall time using 40 computing cores.

3. Aeroservoelastic analysis method

This section outlines the components of the aeroservoelastic analysis, which are based on different disciplinary solvers to simulate the dynamics of the wind turbine. In addition to describing the disciplinary solvers, we also present the aerodynamic and structural design definition, load cases, and applied safety factors.

3.1. Disciplinary solvers

Wind turbines are multidisciplinary systems and thus several disciplinary solvers are needed to simulate the dynamics of the whole system. This paper uses the NREL series of disciplinary solvers, since they are all publicly available. Table 5 lists the solvers used in this work. Details of the wrapping and coupling of these solvers are given by Ashuri et al. [18]

Table 5: Computational codes used simulate the wind turbine aeroservoelastics

Code	Application	Reference
TurbSim	Modeling the flow field	[42]
AeroDyn	Modeling the aerodynamic loading	[43]
AirfoilPrep	Modifying airfoil polar for 3-D effects	[44]
FAST	Modeling the dynamics response of the turbine	[45]
BModes	Computing modal data	[46]
Crunch	Analyzing the time-series	[47]
Fatigue	Computing the fatigue damage	[48]

3.2. Controller design

A variable-speed, variable-pitch-to-feather controller is used in this research. The strategy to control the power production is based on the design of two separable control algorithms [49]: a generator torque controller for the partial and transition load region, and a full-span rotor-collective blade pitch controller for the full load region.

3.3. Aerodynamics and structural design definition

The planform of the blade has nonlinear taper from the maximum chord location at section 6 to the blade tip. The cross section changes from circular in section 1 to an airfoil shape at section 6. The 20 MW turbine uses eight different airfoil types for the blade. The first three airfoils near the root have a circular cross section with a drag coefficients of 0.55 and no lift. The next two airfoils have an elliptic cross section that has a drag coefficient of 0.39, and no lift. The remaining six airfoils are Delft University (DU) and NACA airfoils. Table 6 shows the type and location of all airfoils along the blade.

The airfoils are designed for a Reynolds number of 20 million at the clean condition of the rotor [50]. To do this analysis, we use the airfoil design code RFOIL [51, 52]. Then the methods of Du and Selig [53] and Eggers et al. [54] are used for the rotational stall delay. The drag coefficient is corrected using the method of Viterna and Janetzke [44]. Finally, the Beddoes–Leishman dynamic-stall hysteresis parameters are estimated [55]. AirfoilPrep is used to do these modifications on the airfoil properties (see Table 5) before running the time domain simulations.

The internal structure of the blade consists of a beam box with two spar caps at the bottom and top, and two shear webs between them as shown in Figure 2, with a skin surrounding this box. We made no assumptions about the core, adhesive, bonding, resin, foam and other elements of the blade. However, the contribution of these non-structural elements to the blade properties have implicitly been included, since blade mass and stiffness are dependent on the structural dimensions through a correlation model based on the 5 MW reference turbine.

The tower has a circular cross section along the entire height. Table 7 lists the choice of the materials and their properties for the blade and tower, excluding the safety factors. These data are based on typical values found in engineering literature.

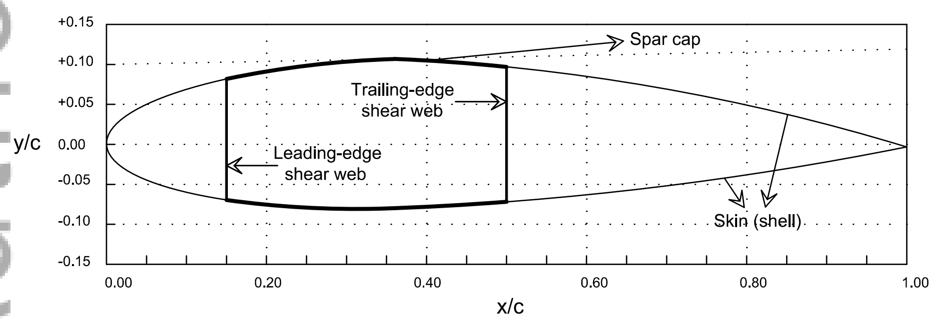

Figure 2: Structural layout of the turbine blade

An analytic model developed by Ashuri et al. [56] is used to obtain the flapwise and edgewise stiffnesses, and the mass per unit length of the blade based on the material

Table 6: Airfoil distribution along the turbine blade span

Section	Airfoil	Distance from root (m)	Pitch axis position (%chord)
1	Circular	0.000	50.0
2	Circular	2.613	50.0
3	Circular	7.020	50.0
4	Elliptic	11.407	46.0
5	Elliptic	15.795	42.0
6	DU00W401	20.182	39.0
7	DU00W401	24.583	37.5
8	DU00W401	28.971	37.5
9	DU00W350	33.358	37.5
10	DU00W350	39.946	37.5
11	DU97W300	53.122	37.5
12	DU91W2250	66.285	37.5
13	DU93W210	79.461	37.5
14	NACA64618	92.623	37.5
15	NACA64618	105.799	37.5
16	NACA64618	118.975	37.5
17	NACA64618	125.550	37.5
18	NACA64618	128.844	37.5
19	NACA64618	132.138	37.5
20	NACA64618	135.000	37.5

properties of Table 7 and the geometry of each cross section. The torsional degree of freedom is assumed to be rigid. These properties are inputs to the aeroelastic solver and used to model the dynamic response of the blade.

A structural damping ratio of 0.477465% (critical in all modes of the isolated blade) that is equal to a 3.0% logarithmic decrement—similar to the 5 MW UpWind turbine—is assumed for the blade in the time domain analysis [4]. For the tower, the structural damping ratio is 1.0% for all the tower modes (first and second of the fore-aft and side-side modes as used for the simulations).

3.4. Design load cases

For the fatigue loads, a normal turbulence model (NTM) is selected for the power production mode, and applied from the cut-in to cut-out wind speed with a reference period of 630 seconds (the first 30 seconds are ignored to ensure that all the transient behaviors are damped out). Since the partial damage contribution from all different directions is accumulated in one direction, the calculated fatigue is an overestimate and yields a conservative design. Such a unidirectional fatigue damage calculation is also allowed based on IEC design standards because it is conservative. Due to this assumption, only the fore-aft fatigue damage at the tower is used as a design constraint, as shown in Table 3.

For extreme loads, DLC 1.3, 2.3, 3.3, 5.1, and 6.1 are considered. Table 8 lists the defined load cases. The IEC-1B class is used for these load cases [57]. For DLC 2.3, an extreme operating gust combined with a grid drop is considered as the fault.

4. Results

In this section, we describe the main design characteristics of the 20 MW wind turbine that resulted from our multidisciplinary design optimization.

4.1. Cost estimation

Table 9 lists the cost and mass data of the 20 MW wind turbine. As the table shows, the LCoE of the 20 MW wind turbine is estimated to be 0.0345 USD/kWhr, with an AEP of 86 GWhr.

4.2. Design variables and constraints

Table 1 lists the initial, optimum, and upper and lower bounds for all the design variables. Linear scaling is employed to find the initial set of design variables. The initial values of the linearly upscaled design variables allow an engineering judgment to be made on the upper and lower bounds of these variables to establish a design space that is neither computationally expensive nor to bounded.

As explained before, we enforce several design constraints. However, only active constraints (those that govern the design) are presented. For the blade, the active constraints are the tip-deflection and fatigue damage at the root. Similarly, for the optimum tower, fatigue is an active constraint, which is typically the case for structures subjected to turbulent wind loading. Further information on the design constraint trends has been detailed in previous work [58, 59, 60, 61, 62, 63]. Table 10 lists the active design constraints for both the blade and tower at the optimum.

4.3. Blade data

Figure 3 shows a schematic view of the wind turbine compared to the largest man-made space rocket, Saturn V, to show the relative scale of the two designs. As the

Table 7: Composite blade and metal tower material properties

Structural element	Young modulus (GPa)	Density (kg/m^3)	Yield stress (MPa)	S–N slope (–)	S–N intercept (MPa)
Blade skin	17	510	276	11	190
Blade web	17	510	276	11	190
Blade spar	32	690	276	11	190
Tower	215	7800	333	5	235

Table 8: Definition of the design load cases based on the IEC standard

Modeled scenario	Load case	Wind speed (m/s)	Yaw error	No. of seeds	Load type
Power generation	1.2	3 to 25	0	9	Fatigue
Power generation	1.3	3 to 25	± 5.6, 0	9	Ultimate
Power generation and fault	2.3	9 to 13, 25	0	6	Ultimate
Start up	3.3	3, 9 to 13, 25	0	3	Ultimate
Emergency shut down	5.1	9 to 13, 25	0	6	Ultimate
Parked situation	6.1	V_{50}	± 8.0, 0	6	Ultimate

figure shows, the 20 MW wind turbine has three 135 m blades. Table 11 presents the blade data. The shown mass distribution adds up to a total blade mass of 259.0 tonnes. The natural frequencies of the blade corresponding to the first and second out-of-plane, and the first in-plane modes are: 0.2860, 1.0032 and 0.6277 Hz, respectively. Figure 4 shows the chord and twist distribution at different stations along the blade. This figure also presents the linearly upscaled blade chord and twist distribution. As the figure shows, the linearly upscaled blade has a uniform distribution compared to the fully nonlinear distribution of the optimized blade.

Figure 5 shows the main aerodynamic properties of the rotor. These aerodynamic properties are obtained by running a series of simulations from the cut-in to cut-out wind speeds assuming a steady wind. The first 60 seconds of the simulations was ignored to ensure that all the transient behaviors were damped out, and the system reaches its steady state status. Using this steady model, a rated wind speed of 10.7 m/s is obtained.

4.4. Drive train data

Table 12 lists the drive train gross properties for the 20 MW wind turbine. The 20 MW design has an optimum rated rotor speed of 7.15 rpm. With a fixed rated generator speed of 1173.7 rpm, a gearbox ratio of 164:1 is needed. Upscaling the properties of the 5 MW UpWind design, results in an equivalent spring constant of 6.94×10^9 Nm/rad, and an equivalent damping constant of 4.97×10^7 Nm/(rad/s) for the drive train.

4.5. Nacelle and hub data

Table 13 presents the optimal gross data of the hub and nacelle. From the mass models developed for the hub, we obtain a mass of 252.8 tonnes. We assume that the hub is made of ductile iron castings and has a spherical shape. Based on the wall thickness of the hub, the hub mass moment of inertia is 2.1×10^6 kg m^2. The nacelle mass (mass of all tower top components except the rotor and hub) is 945.0 tonnes.

Table 9: Cost data for the 20 MW design in 2010 USD

Equipment	Cost ($\times 10^3$ USD)	Mass (tonnes)
Blade	4051.7	259.0
Hub	1456.9	252.8
Pitch system	1945.3	236.0
Hub cone	34.6	4.6
Main shaft	1605.3	159.1
Shaft bearing	1013.4	42.5
Gearbox	4955.5	161.9
Drive train brake	44.4	4.0
Generator	1592.2	59.8
Electronics	1572.8	–
Yaw system	1495.0	176.8
Nacelle frame	752.6	280.8
Nacelle railing	414.2	35.1
Nacelle cover	279.6	23.4
Turbine connection (electrical)	1235.5	–
Cooling and hydraulic system	309.0	1.6
Monitoring and safety system	65.4	–
Tower	3971.0	1588.3
Turbine capital costs (TCC)	34898.2	–
Foundation	290.7	–
Installation	363.1	–
Farm connection (electrical)	838.2	–
Site assessment and permits	934.5	–
Balance of station (BOS)	2426.5	–
Initial capital cost (ICC)	37324.7	–
Levelized replacement cost	249.3	–
Maintenance and operation	108.7	–
Interest rate	0.1185	–
Annual energy production (GWhr)	86.0	–
Levelized cost of energy (USD/kWhr)	0.0345	–

Table 10: Functional constraints of the blade and tower

Description (unit)	Constraint	Optimum
Tip-deflection (m)	≤ 18.3	18.1
Fore-aft fatigue at tower base (-)	≤ 0.70	0.7
Edgewise fatigue at the blade root (-)	≤ 0.70	0.7

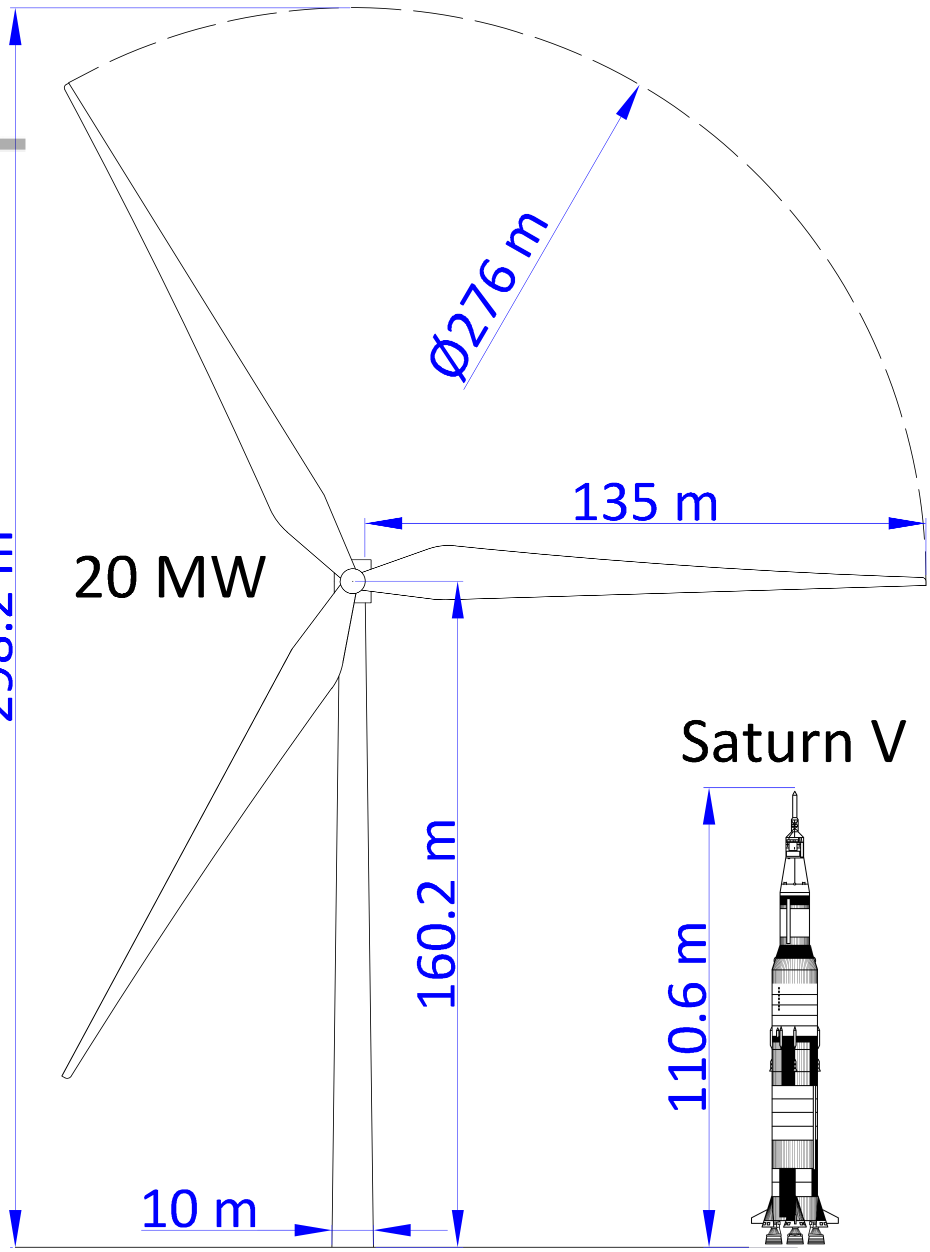

Figure 3: A schematic view of the 20 MW wind turbine and comparison of its size with the Saturn V rocket as the largest space rocket ever made.

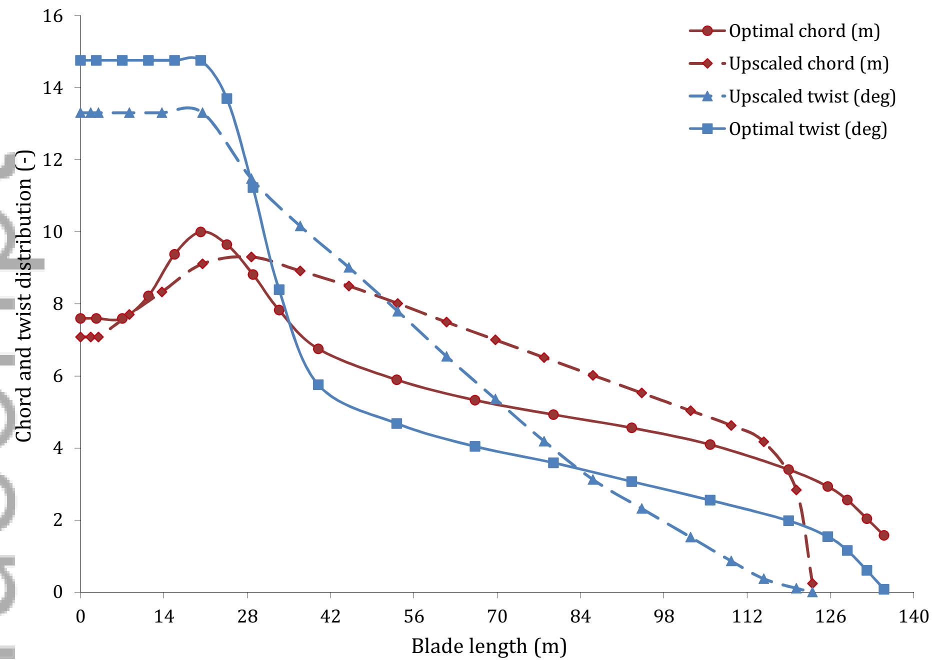

Figure 4: Chord and twist distribution along the span for the linearly upscaled and optimized blades

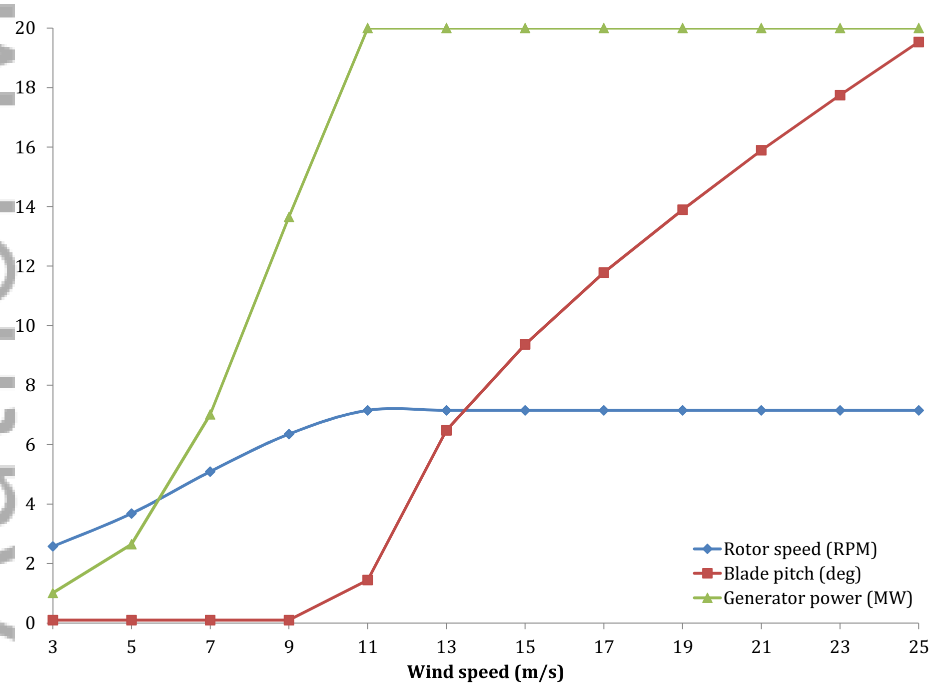

Figure 5: Steady state response for wind speeds form cut-in to cut-out.

Table 11: Blade structural and aerodynamic data

Section No.	Radius (m)	Chord (m)	Twist (deg)	Mass distribution (kg/m^3)	Flap stiffness (Nm^2)	Edge stiffness (Nm^2)
1	0.000	7.600	14.761	2313.552	5.567×10^{11}	5.567×10^{11}
2	2.633	7.600	14.761	2311.491	5.562×10^{11}	5.562×10^{11}
3	7.020	7.600	14.761	4302.129	8.529×10^{11}	9.695×10^{11}
4	11.408	8.222	14.761	4529.572	1.170×10^{12}	1.058×10^{12}
5	15.795	9.378	14.761	4845.071	1.629×10^{12}	1.323×10^{12}
6	20.183	10.000	14.761	3758.496	4.659×10^{11}	9.361×10^{11}
7	24.584	9.650	13.700	3620.345	4.301×10^{11}	8.799×10^{11}
8	28.971	8.819	11.229	2594.361	8.250×10^{10}	4.776×10^{11}
9	33.359	7.829	8.397	2289.785	5.369×10^{10}	3.424×10^{11}
10	39.947	6.755	5.757	1959.583	3.268×10^{10}	2.279×10^{11}
11	53.123	5.895	4.683	1623.365	1.513×10^{10}	1.343×10^{11}
12	66.285	5.330	4.044	1433.568	8.073×10^{9}	1.056×10^{11}
13	79.461	4.928	3.590	1312.959	6.229×10^{9}	8.612×10^{10}
14	92.624	4.560	3.069	1204.471	4.828×10^{9}	7.105×10^{10}
15	105.800	4.095	2.552	1026.201	2.618×10^{9}	4.166×10^{10}
16	118.976	3.403	1.983	842.216	1.470×10^{9}	2.361×10^{10}
17	125.550	2.932	1.541	705.200	9.121×10^{8}	1.460×10^{10}
18	128.844	2.556	1.155	599.282	5.894×10^{8}	9.385×10^{9}
19	132.138	2.039	0.602	464.475	2.910×10^{8}	4.600×10^{9}
20	135.000	1.575	0.081	350.329	1.316×10^{8}	2.061×10^{9}

4.6. Support structure data

The tower and foundation are referred to as the support structure. The soil-structure interaction of the foundation is neglected in this case, and the foundation degrees of freedom at the ground level are constrained to zero. The cost of the foundation system is represented in the design process using engineering models developed by the WindPACT project [26]. These engineering models provide a basis with which the integrity of the design is preserved without loosing too much accuracy in representing the cost.

Table 14 lists the distributed tower properties. The first column lists the location of tower stations measured from the tower base (section 1) to the tower top (section 22) along the tower center-line. Using these data, the first and second natural frequencies of the tower are estimated to be 0.1561 and 1.6802 Hz, respectively. As explained before, the diameter to thickness ratio is constrained to be 160 to avoid buckling.

Table 12: Drive train gross properties for the 20 MW wind turbine

Property	Value (unit)
Rated rotor speed	7.15 (rpm)
Gearbox ratio	164 (-)
Low speed shaft mass	159.1 (tonnes)
Low speed shaft tilt	6.0 (deg)
Gearbox mass	161.9 (tonnes)
High speed shaft coupling and brake mass	4.0 (tonnes)
Generator mass	59.8 (tonnes)
Hydraulic and cooling system mass	1.59 (tonnes)

Table 13: Hub and nacelle data of the 20 MW wind turbine

Property	Value (unit)
Hub height	160.2 (m)
Hub mass	252.8 (tonnes)
Hub cone	4.0 (deg)
Hub mass moment of inertia	2.1×10^6 ($\mathrm{kg} \cdot \mathrm{m}^2$)
Nacelle mass	945.0 (tonnes)
Nacelle mass moment of inertia	7.7×10^7 ($\mathrm{kg} \cdot \mathrm{m}^2$)
Elevation of yaw bearing from tower base	155.0 (m)
Yaw bearing to shaft vertical distance	4.5 (m)
Hub center to yaw axis distance	8.0 (m)

Table 14: Tower data

Section	Height (m)	Diameter (m)	Thickness (m)	Stiffness (Nm^2)
1	0.000	10.000	0.063	5.179×10^{12}
2	3.875	9.918	0.062	5.011×10^{12}
3	11.625	9.748	0.061	4.676×10^{12}
4	19.375	9.571	0.060	4.346×10^{12}
5	27.125	9.388	0.059	4.022×10^{12}
6	34.875	9.197	0.057	3.706×10^{12}
7	42.625	9.000	0.056	3.398×10^{12}
8	50.375	8.788	0.055	3.089×10^{12}
9	58.125	8.559	0.053	2.780×10^{12}
10	65.875	8.321	0.052	2.483×10^{12}
11	73.625	8.080	0.051	2.207×10^{12}
12	81.375	7.845	0.049	1.961×10^{12}
13	89.125	7.622	0.048	1.748×10^{12}
14	96.875	7.420	0.046	1.570×10^{12}
15	104.625	7.233	0.045	1.418×10^{12}
16	112.375	7.053	0.044	1.282×10^{12}
17	120.125	6.880	0.043	1.160×10^{12}
18	127.875	6.714	0.042	1.052×10^{12}
19	135.625	6.556	0.041	9.565×10^{11}
20	143.375	6.406	0.040	8.723×10^{11}
21	151.125	6.266	0.039	7.985×10^{11}
22	155.000	6.200	0.039	7.652×10^{11}

4.7. Controller data

Table 15 lists the gross controller data. Rated rotational speed is the only parameter in this table that is directly optimized. The cut-in and cut-out wind speeds, maximum actuator rate of the pitch mechanism, and generator slip in the transition region (region 21/2) are fixed based on sound engineering judgments. All the other properties and parameters are found based on the optimized design data. As an example, the rated tip-speed is calculated by multiplying the optimized values for rated rotational speed and blade length.

Table 15: Controller data

Property	Value (unit)
Cut-in, rated and cut-out wind speed	3, 10.7, 25 (m/s)
Rated tip-speed	103.3 (m/s)
Peak power coefficient	0.48 (-)
Blade pitch angle at peak power	0.0 (deg)
Rated rotational speed	7.15 (rpm)
Rated mechanical power	21.2 (MW)
Generator slip in transition region	10 (%)
Region 2 torque gain constant	0.11 (N.m/rpm^2)
Maximum actuator rate of the pitch mechanism	4.8 (deg/s)

Figure 6 shows the variation of the PI gains that balance the changes of the aerodynamic power as the wind speed changes. A gain correction factor is used to find the values at any point of interest during operation as presented on the left axis of the graph [49].

5. Conclusion

The design of large wind turbines is a challenging task that calls for innovations in the design methodology. The MDO approach used in the present work is such an innovation. The MDO approach enables aerodynamics, structures, and controls to be integrated to achieve the design of a large wind turbine that has the lowest LCoE and satisfies the design constraints. This is an important step for the development of the future large wind turbines, which must be better designed than they are today in order to reduce costs and make such large turbines economically feasible. This goal was achieved by introducing the LCoE as a common multidisciplinary objective function to minimize, rather than separately optimizing the structure for minimum weight or optimizing aerodynamics for maximum energy output.

The linear scaling law is not adequate in providing feasible and size specific optimized wind turbines that are needed to investigate the technical feasibility and economical characteristic of large scale wind turbines. Nonlinear scaling laws can provide a feasible design that also satisfies all the design constraints, but such a design is far

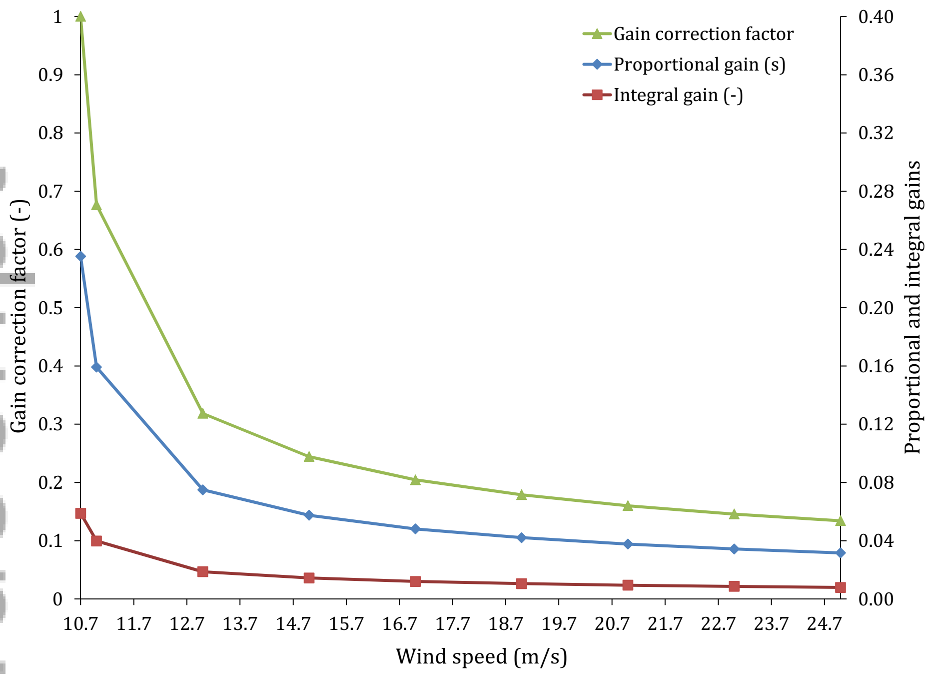

Figure 6: Gain correction and PI gains at different wind turbine operational conditions.

from an optimal design [64, 65]. However, the proposed MDO approach was able to provide a wind turbine optimized for 20 MW power.

In addition, instead of using the traditional methodology to design the tower and rotor separately, the approach of this research enabled the concurrent design of these components. In this work, blade and tower were designed simultaneously resulting in a lower LCoE that if each component were designed separately. This enables the designer to fully understand the technical and economical influence of each component on the design by computing the derivatives of the design constraints and objective function with respect to any variable of interest. This means that the designer can see which variable has the highest impact on any wanted or unwanted function of interest as the design makes progress.

All in all, this has enabled the realization of an optimized 20 MW wind turbine that is feasible, and the results of this research show the technical feasibility of the current wind turbine concept up to 20 MW. Judging from the design constraint values, there seems to be no major technical barrier for this size turbine.

The obtained wind turbine can be used as a baseline design to investigate and compare new technologies or design changes for large turbines, and demonstrate the added value of such turbines. Therefore, the developed 20 MW wind turbine can be used in a similar way as the 5 MW NREL wind turbine is used today by many researchers worldwide. All the corresponding data and simulation files of the common 20 MW research model wind turbine are publicly available to the wind energy community at https://github.com/tashuri/20MW-wind-turbine-model.

6. Future work

We believe that this 20 MW wind turbine design is the first step toward the realization of larger wind turbines, and that the results of this research will allow other researchers to focus on the detailed design of this turbine and improve it further. There are several areas of improvements in this research in order to have reliable future large wind turbines, which we now describe.

To calculate the structural properties of the blade, an analytic technique was employed that did not consider effects such as the bend-twist coupling. A more sophisticated method is recommended for the detailed design of the blade. Buckling is a design issue that needs to be considered for the detailed design of the common 20 MW research model. We also ignored aeroelastic instabilities and soil-foundation interaction, which should be considered at the detailed design stage.

The mass and cost models used for this research are developed for wind turbines at smaller scales. Although these models are well suited for the purpose of this research, they may not be representative of future 20 MW wind turbine. Therefore, we recommended the investigation of new models for larger scale wind turbines.

7. Acknowledgments

The scientific support of Dr. Anthony Waas from the University of Michigan, USA is acknowledged. This research was financially supported by Agentschap NL, under the INNWIND framework.

8. References

[1] Bak C, Bitsche R, Yde A, Kim T, Hansen MH, Zahle F, et al. Light Rotor: The 10-MW reference wind turbine. In: European Wind Energy Conference & Exhibition. 2012, p. 1–10.

[2] Zahle F, Bak C, Guntur S, Sørensen NN, Troldborg N. Comprehensive aerodynamic analysis of a 10 mw wind turbine rotor using 3d cfd. In: 32nd ASME Wind Energy Symposium. 2014, p. 1–15.

[3] Peeringa J, Brood R, Ceyhan O, Engels W, de Winkel G. Upwind 20 MW wind turbine pre-design. Tech. Rep.; ECN, Paper No. ECN-E–11-017; 2011.

[4] van Langen P, Hendrinks B. 5 MW UpWind reference wind turbine data. Tech. Rep.; UpWind internal report; 2010.

[5] Dahlhaug OG, Berthelsen PA, Kvamsdal T, Frøyd L, Gjerde SS, Zhang Z, et al. Specification of the NOWITECH 10 MW reference wind turbine. Tech. Rep.; Norwegian Research Centre for Offshore Wind Technology; 2012.

[6] Frøyd L, Dahlhaug O, et al. Rotor design for a 10 MW offshore wind turbine. In: Proceedings of the Twenty-first International Offshore and Polar Engineering Conference. 2011, p. 19–24.

[7] Muskulus M, Christensen E, Zwick D, Merz K. Improved Tower Design for the NOWITECH 10MW Reference Turbine. In: European Offshore Wind Energy, Frankfurt, Germany. 2013, p. 1–8.

[8] Klair SS. Design of nacelle and rotor hub for NOWITECH 10MW reference turbine. 2013. Master thesis, Norwegian University of Science and Technoloy, Norway.

[9] Bredesen KO. Design of nacelle and yaw bearing for NOWITECH 10 MW reference turbine. 2014. Master thesis, Norwegian University of Science and Technoloy, Norway.

[10] Vatne SR. Aeroelastic instability and flutter for a 10 MW wind turbine. 2011. Master thesis, Norwegian University of Science and Technoloy, Norway.

[11] Frøyd L, Dahlhaug OG, Hansen MH. Prediction of flutter speed on a 10 mw wind turbine. 2011.

[12] Cox K, Echtermeyer A. Structural design and analysis of a 10 MW wind turbine blade. Energy Procedia 2012;24:194–201.

[13] Griffith DT, Ashwill TD. SNL100-00: The Sandia 100-meter all-glass baseline wind turbine blade. Tech. Rep.; Sandia National Laboratories, Albuquerque, Report No. SAND2011-3779; 2011.

[14] Griffith DT. SNL100-01: Carbon design studies for the sandia 100-meter blade. Tech. Rep.; Sandia National Laboratories Technical Report, SAND2013-1178; 2013.

[15] Griffith DT. SNL100-02: Advanced core material design studies for the Sandia 100-meter blade. Tech. Rep.; Sandia National Laboratories Technical Report, SAND2013-10162; 2013.

[16] Griffith DT, Richards PW. Investigating the effects of flatback airfoils and blade slenderness on the design of large wind turbine blades. In: European Wind Energy Association, Barcelona, Spain. 2014, p. 1–8.

[17] Loth E, Ichter B, Selig M, Moriarty P. Downwind pre-aligned rotor for a 13.2 MW wind turbine. 2015.

[18] Ashuri T, Zaaijer MB, Martins JR, van Bussel GJ, van Kuik GA. Multidisciplinary design optimization of offshore wind turbines for minimum levelized cost of energy. Renewable Energy 2014;68:893–905. doi:10.1016/j.renene.2014.02.045.

[19] Fuglsang P, Thomsen K. Site-specific design optimization of 1.5–2.0 MW wind turbines. Journal of solar energy engineering 2001;123(4):296–303.

[20] Maalawi KY, Badr MA. A practical approach for selecting optimum wind rotors. Renewable energy 2003;28(5):803–22.

[21] Méndez J, Greiner D. Wind blade chord and twist angle optimization using genetic algorithms. In: Fifth International Conference on Engineering Computational Technology, Las Palmas de Gran Canaria, Spain. 2006, p. 12–5.

[22] Kenway GKW, Martins JRRA. Aerostructural shape optimization of wind turbine blades considering site-specific winds. In: Proceedings of the 12th AIAA/ISSMO Multidisciplinary Analysis and Optimization Conference. Victoria, BC; 2008, p. 1–12. AIAA 2008-6025.

[23] Xudong W, Shen WZ, Zhu WJ, Sorensen JN, C J. Shape optimization of wind turbine blades. Wind energy 2009;12(8):781–803.

[24] Maki K, Sbragio R, Vlahopoulos N. System design of a wind turbine using a multi-level optimization approach. Renewable Energy 2012;43(12):101–10.

[25] Ashuri T, Zaaijer MB. Review of design concepts, methods and considerations of offshore wind turbines. In: European Offshore Wind Conference and Exhibition, Berlin, Germany. 2007, p. 1–10.

[26] Fingersh L, Hand M, Laxson A. Wind turbine design cost and scaling model. Tech. Rep.; National Renewable Energy Laboratory, NREL/TP-500–40566, Golden, Colorado; 2006.

[27] Poore R, Lettenmaier T. Alternative design study report: WindPACT Advanced wind turbine drive train designs study. Tech. Rep.; National Renewable Energy Laboratory, NREL/SR-500-33196, Golden, CO.; 2003.

[28] Griffin DA. Windpact turbine design scaling studies technical area 1: Composite blades for 80-to 120-meter rotor. Tech. Rep.; National Renewable Energy Laboratory, NREL/SR-500-29492, Golden, CO.; 2001.

[29] Smith K. Windpact turbine design scaling studies technical area 2: Turbine, rotor, and blade logistics. Tech. Rep.; National Renewable Energy Laboratory, NREL/SR-500-29439, Golden, CO.; 2001.

[30] Bywaters G, John V, Lynch J, Mattila P, Norton G, Stowell J, et al. Northern power systems windpact drive train alternative design study report; period of performance: April 12, 2001 to January 31, 2005. Tech. Rep.; National Renewable Energy Laboratory, NREL/SR-500-35524, Golden, CO.; 2004.

[31] Shafer D, Strawmyer K, Conley R, Guidinger J, Wilkie D, Zellman T, et al. Windpact turbine design scaling studies: Technical area 4–balance-of-station cost. Tech. Rep.; National Renewable Energy Laboratory, NREL/SR-500-29950, Golden, CO.; 2001.

[32] Brand AJ. Offshore wind atlas of the Dutch part of the North sea. Tech. Rep.; ECN-M-09-050, Energy research Centre of the Netherlands, Petten; 2008.

[33] Martins JRRA, Lambe AB. Multidisciplinary design optimization: A survey of architectures. AIAA Journal 2013;51(9):2049–75. doi:10.2514/1.J051895.

[34] Lambe AB, Martins JRRA. Extensions to the design structure matrix for the description of multidisciplinary design, analysis, and optimization processes. Structural and Multidisciplinary Optimization 2012;46:273–84. doi:10.1007/s00158-012-0763-y.

[35] Nijssen R, Zaaijer M, Bierbooms W, Van Kuik G, Van Delft D, van Holten T. The application of scaling rules in up-scaling and marinisation of a wind turbine. In: European Wind Energy Conference and Exhibition (EWEC). 2001, p. 1–4.

[36] Teng JG, Rotter JM. Buckling of thin metal shells. CRC Press; 2006.

[37] Bhattacharya S, Carrington T, Aldridge T. Buckling considerations in pile design. In: ISFOG: Frontiers in Offshore Geotechnics. 2005, p. 815–21.

[38] Ashuri T. Beyond classical upscaling: Integrated aeroservoelastic design and optimization of large offshore wind turbines. PhD thesis; Delft University of Technology; the Netherlands; 2012.

[39] Kooijman H, Lindenburg C, Winkelaar D, Van der Hooft E. DOWEC 6 MW pre-design: Aero-elastic modelling of the DOWEC 6 MW pre-design in PHATAS. Tech. Rep.; DOWEC Dutch Offshore Wind Energy Converter 1997–2003 Public Reports; 2003.

[40] Fleury C. CONLIN: An efficient dual optimizer based on convex approximation concepts. Structural and Multidisciplinary Optimization 1989;1(2):81–9.

[41] Birgin EG, Martinez JM. Improving ultimate convergence of an augmented Lagrangian method. Optimization Methods and Software 2008;23(2):177–95.

[42] Jonkman BJ, Buhl ML. Turbsim user's guide. Tech. Rep.; National Renewable Energy Laboratory, NREL/TP-500–41136, Golden, Colorado; 2007.

[43] Laino DJ, Hansen AC. User's guide to the wind turbine dynamics aerodynamics computer software AeroDyn. Tech. Rep.; Windward Engineering LLC, Prepared for the National Renewable Energy Laboratory under Subcontract No. TCX-9-29209-01, Salt Lake City, UT; 2002.

[44] Viterna LA, Janetzke DC. Theoretical and experimental power from large horizontal-axis wind turbines. Tech. Rep.; National Aeronautics and Space Administration, Cleveland, OH (USA). Lewis Research Center; 1982.

[45] Jonkman JM, Buhl ML. FAST user's guide. Tech. Rep.; National Renewable Energy Laboratory, NREL/EL-500–29798, Golden, Colorado; 2004.

[46] Bir GS. User's guide to BModes. Tech. Rep.; National Renewable Energy Laboratory, NREL/TP-500–39133, Golden, Colorado; 2007.

[47] Buhl ML. Crunch user's guide. Tech. Rep.; National Renewable Energy Laboratory, NREL/EL-500–30122, Golden, Colorado; 2003.

[48] Frendahl M, Rychlik I. Rainflow analysis: Markov method. International journal of fatigue 1993;15(4):265–72.

[49] Ashuri T, Zaaijer MB, van Bussel GJW, van Kuik GAM. Controller design automation for aeroservoelastic design optimization of wind turbines. In: The science of making torque from wind, Crete, Greece. 2010, p. 1–7.

[50] Ashuri T, Rotea M, Xiao Y, Li Y, Ponnurangam CV. Wind turbine performance decline and its mitigation via extremum seeking controls. In: 34^{th} wind energy sympossium. American Institute of Aeronautics and Astronautics, AIAA; 2016, p. 1–11.

[51] Van Rooij R, Timmer W. Roughness sensitivity considerations for thick rotor blade airfoils. Journal of solar energy engineering 2003;125(4):468–78.

[52] Timmer W, Schaffarczyk A. The effect of roughness at high reynolds numbers on the performance of aerofoil du 97-w-300mod. Wind Energy 2004;7(4):295–307.

[53] Du Z, Selig M. A 3-D stall-delay model for horizontal axis wind turbine performance prediction. In: AIAA-98-0021. 1998, p. 9–21.

[54] Eggers AJ, Chaney K, Digumarthi R, Incorporated R. An assessment of approximate modeling of aerodynamic loads on the UAE rotor. In: 41st Aerospace Sciences Meeting and Exhibit, Reno, NV. 2003, p. 6–9.

[55] Leishman JG, Beddoes TS. A semi-empirical model for dynamic stall. Journal of the American Helicopter Society 1989;34(3):3–17.

[56] Ashuri T, Zaaijer MB, van Bussel GJW, van Kuik GAM. An analytical model to extract wind turbine blade structural properties for optimization and up-scaling studies. In: The science of making torque from wind, Crete, Greece. 2010, p. 1–7.

[57] IEC61400 . Wind turbines, part 3: Design requirements for offshore wind turbines. 2009.

[58] Ashuri T, van Bussel GJW, Mieras S. Development and validation of a computational model for design analysis of a novel marine turbine. Wind Energy 2013;16(1):77–90. doi:10.1002/we.530.

[59] van der Meulen MB, Ashuri T, van Bussel GJW, Molenaar DP. Influence of nonlinear irregular waves on the fatigue loads of an offshore wind turbine. In: The Science of Making Torque from Wind, Oldenburg, Germany. 2012, p. 1–10. doi:10.13140/2.1.3034.5606.

[60] Haghi R, Ashuri T, van der Valk PL, Molenaar DP. Integrated multidisciplinary constrained optimization of offshore support structures. In: The science of Making torque from wind; vol. 555. Journal of Physics, 555 012046; 2012, p. 1–10. doi:10.1088/1742-6596/555/1/012046.

[61] Muskulus M. The full-height lattice tower concept. Energy Procedia 2012;24:371–7.

[62] de Vries W, Vemula NK, Passon P, Fischer T, Kaufer D, Matha D, et al. Final report wp4. 2: Support structure concepts for deep water sites. Tech. Rep.; UpWind project; 2011.

[63] Van Der Tempel J. Design of support structures for offshore wind turbines. PhD thesis; Delft University of Technology; the Netherlands; 2006.

[64] Capponi PC, Ashuri T, van Bussel GJW, Kallesøe B. A non-linear upscaling approach for wind turbine blades based on stresses. In: European Wind Energy Conference and Exhibition, Brussels, Belgium. European Academy of Wind Energy; 2011, p. 1–8.

[65] Ashuri T, Zaaijer MB. Size effect on wind turbine blade's design drivers. In: European Wind Energy Conference and exhibition, Brussels, Belgium. 2008, p. 1–6.